Contact-Free Pedestrian Tracking Using Massive MIMO-OFDM Communication System

Chenglong Li[†1], Sibren De Bast[‡2], Yang Miao[‡♯3], Emmeric Tanghe[†4], Sofie Pollin[‡5], Wout Joseph[†6]

[†]WAVES group, Department of Information Technology, Ghent University-imec, 9052 Ghent, Belgium

[‡]Department of Electrical Engineering, KU Leuven, 3000 Leuven, Belgium

[♯]Faculty of Electrical Engineering, Mathematics and Computer Science (EEMCS), University of Twente, 7522 Enschede, The Netherlands

{[1]chenglong.li,[4]emmeric.tanghe,[6]wout.joseph}@ugent.be, {[2]sibren.debast,[5]sofie.pollin}@kuleuven.be, {[3]y.miao}@utwente.nl

***Abstract*— This paper establishes an indoor distributed radar-like prototype using a sub-6 GHz massive multiple-input multiple-output (MIMO) communication system. Based on the prototype, the contact-free human tracking performance is experimentally evaluated. Instead of extracting the location related geometrical metrics (angle and distance), we propose to localize the pedestrian through the channel state information (CSI) directly. Inspired by the concept of synthetic aperture, a particle filter-based hologram tracking algorithm is proposed. The experimental results show that the proposed algorithm can achieve 20.1-cm mean tracking accuracy in real-time.**

***Keywords*— Massive multiple-input multiple-output, indoor localization, wireless sensing, synthetic aperture radar, channel state information.**

I. Introduction

Human activity recognition (HAR) has attracted extensive attention in the past decade due to its potential application in areas such as elderly care, smart homes, virtual reality, etc. Especially, the radio frequency (RF) based contact-free (*a.k.a.*, device-free or passive) human sensing becomes an active research area as there is no user-attached sensor needed and there are less privacy concerns compared to the vision-based solutions. During the last five years, numerous passive sensing techniques have been proposed based on different RF standards and hardware, including radio frequency identification (RFID) [1], ultra-wideband (UWB) [2], Bluetooth low energy (BLE), WiFi [3], [4], millimeter-wave [5], etc. As a milestone of the fifth-generation (5G) wireless communication, the massive multiple-input multiple-output (MIMO) technique not only improves communication in terms of channel capacity and spectral efficiency but also has the potential for accurate location-based services (LBS) due to the high spatial resolution [6], [7], [8]. Jointly motivated by recent advances in hardware and signal processing, sensing functionality can be integrated into wireless communication networks allowing to reuse the spectrum, hardware, and even signaling resources, and achieving so-called integrated sensing and communication [9].

In this paper, we investigate indoor contact-free human tracking exploiting a massive MIMO communication system. Inspired by the concept of radio stripe (cell-free massive MIMO [10]), we implement the distributed massive MIMO radar-like system with the large antenna array separated in an indoor environment. On the basis of the prototype, we conduct the contact-free pedestrian tracking experiment. A synthetic aperture-based algorithm is proposed, which localizes the target in real-time from the channel response directly and does not require intermediate geometrical metrics (angle and distance) compared with other common solutions.

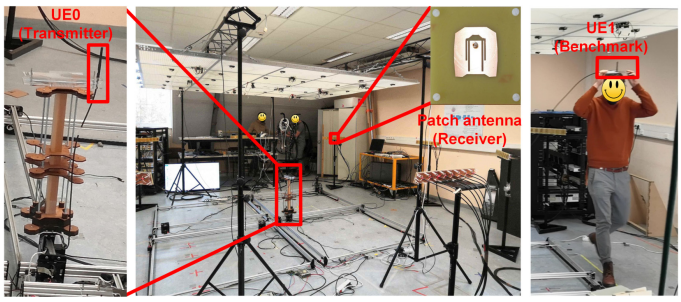

Fig. 1. Measurement setups of the distributed massive MIMO radar-like system. User equipment (UE0, transmitter) is deployed in the center of the targeted area. The receiver consists of 64 patch antennas. UE1 on the top of participant's head is used for active tracking (benchmark).

II. Experiment and Data Pre-processing

A. Measurement Campaign

In this section, we introduce the measurement campaign for the radar-like pedestrian tracking based on the massive MIMO testbed at KU Leuven ESAT-WAVECORE, as shown in Fig. 1. The Massive MIMO system is built on time division duplex (TDD)-based orthogonal frequency-division multiplexing (OFDM) signaling, following the NI Labview Application Framework [11]. For the tracking purpose in this paper, only the uplink procedure has been considered, *i.e.*, the base station (BS) receives the orthogonal pilots sent by the transmitter (user equipment, UE) and conducts the channel estimation to obtain the channel state information (CSI). The CSI sampling rate is 100 Hz, the center frequency is 2.61 GHz, and the bandwidth is 18 MHz with 100 evenly-spaced sub-carriers. The massive antennas of the BS have been deployed as 8 distributed uniform linear arrays (ULA) of 1×8 antennas, as shown in Fig. 2. The adjacent antenna elements of the short ULAs are spaced by 7 cm and the height is 1.205 m. The transmitter (UE0) uses a single dipole antenna with a height of 0.8 m, which is fixed in the center of the target area.

https://doi.org/10.23919/EuRAD54643.2022.9924658

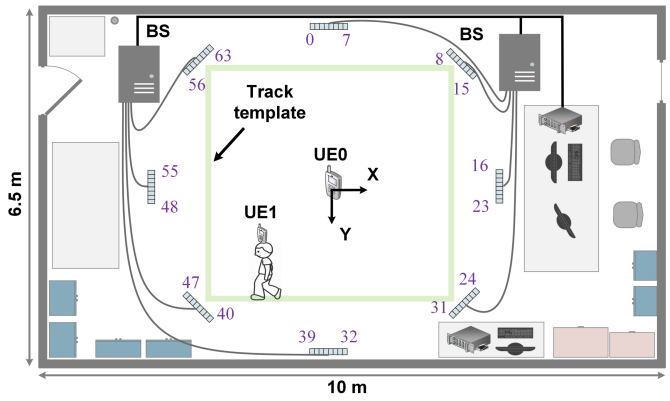

Fig. 2. Floor plan of the distributed massive MIMO radar-like pedestrian tracking experiment. The large antenna array of BS is separated into 8 short ULAs (8×1), together with UE0, which consists of the indoor distributed radar system. The green rectangular is the predefined pedestrian track template.

For the contact-free human tracking, the communication links established between the distributed BSs and UE form a sensing zone where the device-free walking human can be localized and tracked via characterizing the reflected/scattered signals on the body. In the experiment, we have predefined a rectangular track template for the person to walk. Three persons participated in the experiment and each person walked counterclockwise along the designed template first, and then walked clockwise, as in Fig. 2. However, it should be noted that it is not possible for the participants to follow exactly the template track due to distinct individual movements. To handle this problem, we have asked for each participant to carry an additional transmitter (*i.e.*, UE1) for active tracking to determine a "ground truth". To avoid the possible body shadowing effect, we have placed the antenna on the top of the participant's head, as shown in Fig. 2. In this paper, we regard the active tracking results as the benchmark for radar-like (contact-free) tracking. The positioning accuracy of the active tracking will be validated in Section III-C.

B. CSI Calibration

Due to the imperfect synchronization and hardware signal processing, the measured raw CSI suffers from various frequency-dependent phase errors, including the sampling frequency offset (SFO), symbol timing offsets (STO), in-phase quadrature-phase (IQ) imbalance, etc [8], [12]. Moreover, resulting from the heterogeneity of hardware components, there are constant phase offsets among each antenna element of massive MIMO BS. Note that we do not consider the antenna coupling effect here. The phase errors in the frequency domain and antenna domain make the CSI intractable for positioning and tracking purposes. To this end, we need to calibrate the massive MIMO prototype before the radar experiment. During the calibration, the UE is placed at different locations (the number of locations is no less than the number of antenna elements of BS [8]). We have used a computerized numerical control (CNC) X-Y table (mm-level accuracy) to provide the ground truth of the UE's locations. The idea of CSI pre-processing is to calibrate the frequency-dependent errors at each antenna element first, and then use the residual phase after the removal of frequency-dependent phase offsets to align the phases along the antenna array. After this, we save the parameters needed for CSI calibration and utilize these parameters to calibrate the CSI in the radar experiment directly. Due to the page limitation, we omit the details here and recommend the readers to refer to [8] for the detailed analysis and implementation.

III. Synthetic Aperture for Human Tracking

A. Target-of-Interest

In case the pedestrian is walking in an indoor scenario, the received signal portrays the multipath components (MPCs) via the CSI at time t and frequency f (in equivalent baseband),

$$H(t,f)=\sum_{i\in\mathcal{S}}\alpha_i(f)e^{-\mathcal{J}2\pi\frac{d_i}{\lambda}}+\sum_{j\in\mathcal{D}}\alpha_j(t,f)e^{-\mathcal{J}2\pi\left(\frac{d_{n_r}^{(j)}(t)}{\lambda}+\nu_{n_r}^{(j)}t\right)}, \tag{1}$$

where $\mathcal{S}$ and $\mathcal{D}$ represent the MPCs of the static objects (the direct link and reflections/scattering from surroundings) and the dynamic target, respectively. $\alpha_{(\cdot)}$, $d_{(\cdot)}$, and $\nu_{(\cdot)}$ denote the complex gain, link length, and Doppler shift, respectively. $\mathcal{J}=\sqrt{-1}$. In the framework of pedestrian tracking, the target of interest (TOI) is the components reflected/scattered from the moving person. In this paper, we use a simple yet efficient static components removal method. Specifically, we adopt a moving average method to obtain the mean CSI within a slow-time sliding window. Given the fact that the reflected power from the human body is much weaker than the direct link and many of the static reflections, we can remove most of the static components using the mean subtraction. To handle the residual interference, we propose to use the Doppler frequency shift (DFS) to refine the TOI. Define the CSI after the mean subtraction as $\mathbf{H}=\{H_{n_r,n_k,n_t}\}\in\mathbb{C}^{N_r\times N_k\times N_t}$, where N_r, N_k, N_t denote the number of BS antenna elements, sub-carriers, and CSI samples within the a short (slow) time window, respectively. The time window is set as 0.1 s in which we presume the change of pedestrian's location is negligible.

Note that for the distributed massive MIMO within an indoor scenario, the DFS at the large antenna array may be significant. So, we estimate the DFS for each antenna element separately. Define the N_{D}-point discrete Fourier transform (DFT) matrix $\mathbb{D}_{N_t\times N_{\mathrm{D}}}$ and the N_{T}-point DFT matrix $\mathbb{T}_{N_k\times N_{\mathrm{T}}}$, given by, respectively,

$$[\mathbb{D}_{N_t\times N_{\mathrm{D}}}]_{n_t,n_{\mathrm{D}}}=\frac{1}{\sqrt{N_{\mathrm{D}}}}\left(e^{-\mathcal{J}2\pi/N_{\mathrm{D}}}\right)^{(n_t-1)(n_{\mathrm{D}}-1)},$$
$$[\mathbb{T}_{N_k\times N_{\mathrm{T}}}]_{n_k,n_{\mathrm{T}}}=\frac{1}{\sqrt{N_{\mathrm{T}}}}\left(e^{-\mathcal{J}2\pi/N_{\mathrm{T}}}\right)^{(n_k-1)(n_{\mathrm{T}}-1)}.$$

Define the CSI after mean subtraction for the n_r-th antenna element as $\mathbf{H}_{n_r}\in\mathbb{C}^{N_k\times N_t}$. So the range-Doppler profile at the n_r-th antenna is given by $\hat{\mathbf{H}}_{n_r}=\mathbb{T}^{\mathrm{H}}\mathbf{H}_{n_r}\mathbb{D}\in\mathbb{C}^{N_{\mathrm{T}}\times N_{\mathrm{D}}}$. We can obtain the TOI, given by $[\hat{\mathbf{H}}_{\mathrm{TOI}}]_{n_r}=\hat{h}_{n_r}=\hat{\mathbf{H}}_{n_r}(\hat{n}_{\mathrm{T}},\hat{n}_{\mathrm{D}})$,

$$(\hat{n}_{\mathrm{T}},\hat{n}_{\mathrm{D}})=\arg\max_{n_{\mathrm{T}},n_{\mathrm{D}}}\mathbb{E}\left\{(\mathbb{T}^{\mathrm{H}}\mathbf{H}_{n_r}\mathbb{D})\odot(\mathbb{T}^{\mathrm{H}}\mathbf{H}_{n_r}\mathbb{D})^*\right\}, \tag{2}$$

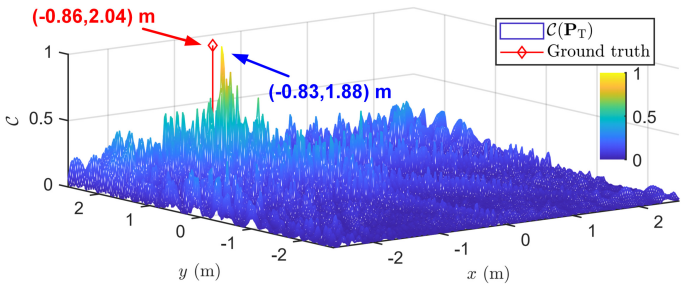

Fig. 3. Synthetic aperture for the distributed massive MIMO radar: The maximal $\mathcal{C}(\mathbf{P}_\mathrm{T})$ identifies the estimated location of the pedestrian, namely $(-0.83, 1.88)$m, whereas the ground truth is $(-0.86, 2.04)$m.

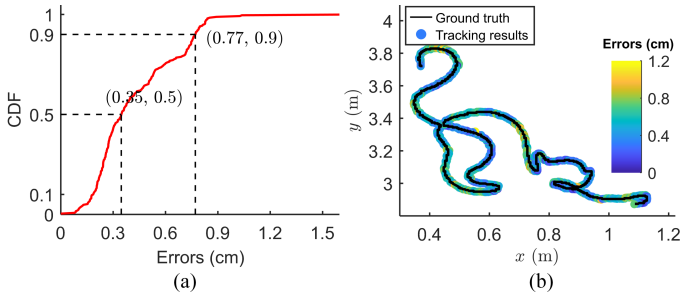

Fig. 4. Benchmarking: active human tracking results based on the distributed massive MIMO system. (a) CDF of tracking errors based on CNC X-Y table. (b) Tracking results of a "*cat-shape*" trajectory using the open-access massive MIMO dataset in [13].

where $\odot$ denotes the Hadamard product.

B. Synthetic Aperture

Tracking the pedestrian based on the distance and angle information generally requires complex high-order parameters estimation algorithm [4], such as space alternating generalized expectation maximization (SAGE). However, in this section, we propose to track the pedestrian based on the received phase directly, as the phase is sensitive to the finer-grained distance changing, which makes it promising for the positioning purpose, especially for the sub-6 GHz systems [7]. Define the phase of TOI of the n_r-th antenna as $\phi_{n_r} = 2\pi\frac{d_{n_r}}{\lambda} + \phi_0$, where ϕ_0 is the constant phase offsets caused by the hardware. d_{n_r} is the reflected distance, given by $d_{n_r} = \|\mathbf{P}_\mathrm{T} - \mathbf{P}_\mathrm{UE0}\| + \|\mathbf{P}_\mathrm{T} - \mathbf{P}_{n_r}\|$, where $\mathbf{P}_\mathrm{T}$, $\mathbf{P}_\mathrm{UE0}$, and $\mathbf{P}_{n_r}$ are the coordinates of the target, transmitter, and the n_r-th antenna of receiver, respectively. Define the measured phase of TOI of n_r-th antenna as $\phi_{n_r}^{(m)} = \angle\hat{h}_{n_r}$ and amplitude $\alpha_{n_r}^{(m)} = |\hat{h}_{n_r}|$. Stemming from the concept of synthetic aperture radar (SAR), the location of the target $\hat{\mathbf{P}}_\mathrm{T}$ can be estimated via,

$$\begin{aligned}\arg\max_{\mathbf{P}_\mathrm{T}} \mathcal{C}(\mathbf{P}_\mathrm{T}) &= \arg\max_{\mathbf{P}_\mathrm{T}} \left| \sum_{n_r=1}^{N_r} \alpha_{n_r}^{(m)} e^{-\mathcal{J}\left(\phi_{n_r}^{(m)} - (2\pi\frac{d_{n_r}}{\lambda} + \phi_0)\right)} \right| \\ &= \arg\max_{\mathbf{P}_\mathrm{T}} \left| \sum_{n_r=1}^{N_r} \alpha_{n_r}^{(m)} e^{\mathcal{J}\left(2\pi\frac{d_{n_r}}{\lambda} - \phi_{n_r}^{(m)}\right)} \right|. \end{aligned} \tag{3}$$

Since $\mathcal{C}(\mathbf{P}_\mathrm{T})$ in (3) is nonlinear and nonconvex, a common solution to obtain $\hat{\mathbf{P}}_\mathrm{T}$ is conducting the grid search within the targeted area and find the index of the maximum, as shown in Fig. 3. However, the global grid search is extremely time-consuming, especially for a large targeted area and a small searching step. To handle this problem, we propose to estimate the target's location via tracking the changes of $\mathcal{C}(\mathbf{P}_\mathrm{T})$ based on particle filter (PF) algorithm. The grid search is just used for initialization. For each location update, the candidate region is constrained by the human motion model, given by,

$$\begin{bmatrix} \mathbf{P}_\mathrm{T}^{(t+1)} \\ \mathbf{v}_\mathrm{T}^{(t+1)} \end{bmatrix} = \begin{bmatrix} \mathbf{I}_2 & \Delta t \cdot \mathbf{I}_2 \\ \mathbf{0} & \mathbf{I}_2 \end{bmatrix} \begin{bmatrix} \mathbf{P}_\mathrm{T}^{(t)} \\ \mathbf{v}_\mathrm{T}^{(t)} \end{bmatrix} + \begin{bmatrix} \Delta t \cdot \mathbf{1}_{2\times 1} \\ \mathbf{1}_{2\times 1} \end{bmatrix} n_v, \tag{4}$$

where $\mathbf{v}_\mathrm{T}$ is the velocity of the moving target. Δt is the time difference between two consecutive timestamps. n_v is the Gaussian velocity errors. We can thus avoid the global search for each updating of new measurement and speed up the computation. The updated particles are weighted via the differences compared with the maximum of $\mathcal{C}(\mathbf{P}_\mathrm{T}^{(i)})$ [2]

$$\begin{aligned} \hat{P}_w^{(i)} &= \exp\left(\frac{1}{2\sigma_c^2}\left(\min_{1\le i\le K}\left\{P_w^{(i)}\right\} - P_w^{(i)}\right)\right), \\ P_w^{(i)} &= \left(\mathcal{C}_\mathrm{max} - \mathcal{C}(\mathbf{P}_\mathrm{T}^{(i)})\right)^2, \end{aligned} \tag{5}$$

where K is the number of particles and σ_c the standard deviation of $\mathcal{C}$. Note that $\mathcal{C}_\mathrm{max} = 1$ because we normalize $\mathcal{C}(\mathbf{P}_\mathrm{T})$ to $(0, 1]$.

C. Benchmark: Active Tracking

As mentioned in Section II-A, we adopt the positioning results of active tracking as the benchmark ("ground truth") for our radar-like tracking. For the active tracking, we have also utilized a similar SAR-based solution as in Section III-B but used the received phase directly without static components removal. To validate the feasibility of active tracking as the benchmark, we evaluate the positioning accuracy of active tracking using the collected data based on the CNC X-Y table, which can provide the mm-level location ground truth. Fig. 4(a) shows the cumulative distribution functions (CDF) of the tracking errors. The distributed massive MIMO system can guarantee sub-centimeter level tracking accuracy despite some outliers (50th percentile errors 0.35 cm and 90th percentile errors 0.77 cm). Moreover, we have also evaluated the active tracking accuracy using our previous dense distributed massive MIMO dataset (open-access in [13]). We formulate the tracking trajectory as a "*cat shape*", as shown in Fig. 4(b). The tracking results show that a comparable accuracy can be achieved, which also indicates the feasibility of active tracking as the benchmark for the radar-like scheme.

IV. Performance Evaluation

In this section, we evaluate the performance of contact-free human tracking using the sub-6 GHz distributed massive MIMO communication testbed. Fig. 5 shows that the radar-like prototype achieves 20.1-cm mean errors for three participants compared with the active tracking (benchmark), and maximal tracking errors of 40 to 45 cm in spite of some outliers. The

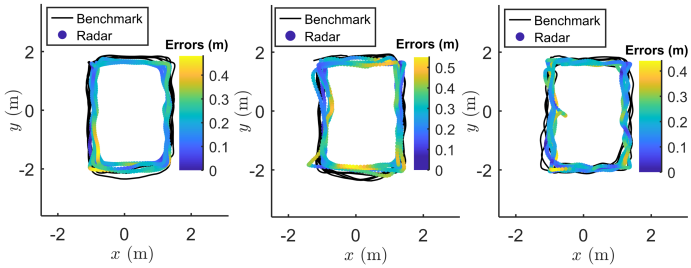

Fig. 5. Massive MIMO radar-like tracking results corresponding to three participants and the comparison with the active tracking results (benchmark).

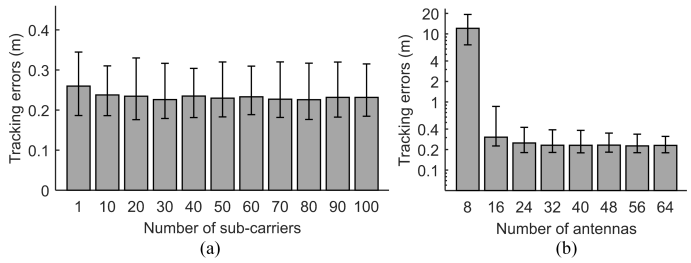

Fig. 6. Massive MIMO radar-like 75th percentile tracking errors with low bound 50th percentile and upper bound 95th percentile errors: (a) Impact of the number of sub-carriers. (b) Impact of the number of antennas.

achievable performance is sufficient for pedestrian tracking considering the size of the human body (with a radius of 20 to 30 cm under the cylindrical body model hypothesis).

Moreover, we introduce the PF algorithm in Section III-B instead of conducting the grid search, so the location inference time for each update is short. In the algorithm, we set the number particles as $K = 2000$, $N_{\mathrm{D}} = 256$, $N_{\mathrm{T}} = 64$, and the running environment is Dell OptiPlex 7050 with an Intel(R) Core(TM) i7-7700 CPU@3.60GHz and 16 GB RAM. The average inference time for each location update is about 37.4 ms, which is much smaller than the slow-time window of 100 ms adopted for the location updating. This shows that the proposed algorithm can ensure accurate tracking in real-time.

Fig. 6 evaluates the tracking performance with respect to the impact of bandwidth and number of antennas. The tracking errors in Fig. 6(a) fluctuate slightly (about 2 cm) and the performance has no degradation even if a single sub-carrier has been adopted. Furthermore, as shown in Fig. 6(b), increasing the number of the antenna elements improves the tracking accuracy and reduces the outliers distinctly. Nevertheless, the accuracy saturates when the number of antennas reaches 24 for this experiment. Note that for evaluating the impact of the number of antennas, we did not optimize the antenna placement but simply increased them sequentially, as the labeled order shown in Fig. 2. When the antenna number is 8, we observe extremely large tracking errors. It is because the selected 8 antennas are co-located which has a limited size of synthetic aperture.

V. Conclusion and Future Work

In this paper, we investigated radar-like pedestrian tracking using a sub-6 GHz distributed massive MIMO communication testbed. Taking advantage of the synthetic aperture, we proposed to localize the target using CSI directly without the requirement of intermediate geometrical metrics (distance and angle). We introduced a particle filter to avoid time-consuming global search and achieved 20.1-cm mean tracking accuracy in real-time. The future works will consist of multi-target tracking and finer-grained limb tracking.

Acknowledgment

This work is supported in part by the Excellence of Science (EOS) project MUlti-SErvice WIreless NETworks (MUSE-WINET), by the Research Foundation Flanders (FWO) SB Ph.D. fellowship under Grant 1SA1619N, and by the FWO project under Grant G098020N.

References

[1] C. Dian, D. Wang, Q. Zhang, R. Zhao, and Y. Yu, "Towards domain-independent complex and fine-grained gesture recognition with RFID," *Proceedings of the ACM on Human-Computer Interaction*, vol. 4, no. ISS, pp. 1–22, 2020.

[2] C. Li, E. Tanghe, L. Martens, J. Romme, G. Singh, E. De Poorter, and W. Joseph, "Device-free pedestrian tracking using low-cost ultra-wideband devices," *IEEE Trans. Instrum. Meas.*, vol. 71, pp. 1–4, 2022.

[3] D. Wu, D. Zhang, C. Xu, H. Wang, and X. Li, "Device-free WiFi human sensing: From pattern-based to model-based approaches," *IEEE Commun. Mag.*, vol. 55, no. 10, pp. 91–97, 2017.

[4] K. Qian, C. Wu, Y. Zhang, G. Zhang, Z. Yang, and Y. Liu, "Widar2.0: Passive human tracking with a single Wi-Fi link," in *Proceedings of the 16th Annual International Conference on Mobile Systems, Applications, and Services*, Jun 2018, pp. 350–361.

[5] X. Yang, J. Liu, Y. Chen, X. Guo, and Y. Xie, "MU-ID: Multi-user identification through gaits using millimeter wave radios," in *IEEE INFOCOM 2020-IEEE Conference on Computer Communications*. IEEE, 2020, pp. 2589–2598.

[6] E. Björnson, L. Sanguinetti, H. Wymeersch, J. Hoydis, and T. L. Marzetta, "Massive MIMO is a reality—what is next?: Five promising research directions for antenna arrays," *Digital Signal Processing*, vol. 94, pp. 3–20, 2019.

[7] X. Li, E. Leitinger, M. Oskarsson, K. Åström, and F. Tufvesson, "Massive MIMO-Based Localization and Mapping Exploiting Phase Information of Multipath Components," *IEEE Trans. Wireless Commun.*, vol. 18, no. 9, pp. 4254–4267, Sep 2019.

[8] C. Li, S. De Bast, E. Tanghe, S. Pollin, and W. Joseph, "Towards fine-grained indoor localization based on massive MIMO-OFDM system: Experiment and analysis," *IEEE Sensors J.*, vol. 22, no. 6, pp. 5318–5328, 2022.

[9] C. De Lima, et al., "Convergent communication, sensing and localization in 6G systems: An overview of technologies, opportunities and challenges," *IEEE Access*, vol. 9, pp. 26 902–26 925, 2021.

[10] G. Interdonato, E. Björnson, H. Quoc Ngo, P. Frenger, and E. G. Larsson, "Ubiquitous cell-free massive MIMO communications," *EURASIP Journal on Wireless Communications and Networking*, vol. 2019, no. 1, pp. 1–13, 2019.

[11] National Instrument, "5G Massive MIMO Testbed: From Theory to Reality," [Online] https://www.ni.com/nl-be/innovations/white-papers/14/5g-massive-mimo-testbed--from-theory-to-reality--.html, Mar 2019.

[12] H. Zhu, Y. Zhuo, Q. Liu, and S. Chang, "π-Splicer: Perceiving Accurate CSI Phases with Commodity WiFi Devices," *IEEE Trans. Mobile Comput.*, vol. 17, no. 9, pp. 2155–2165, Sep 2018.

[13] S. De Bast and S. Pollin, "Ultra Dense Indoor MaMIMO CSI Dataset," [IEEE Dataport]. Available: https://dx.doi.org/10.21227/nr6k-8r78, Feb 2021.